Journal of Sciences, Islamic Republic of Iran 29(4): 321 - 333 (2018) http://jsciences.ut.ac.ir
University of Tehran, ISSN 1016-1104

Inorganic Complex Precursor: Preparation of Cu-Mn/SiO_2 Mixed Oxide Nanocatalyst for Low-Temperature Water-Gas Shift Reaction

J. Farzanfar, A. R. Rezvani*

Department of Chemistry, Faculty of Sciences, University of Sistan and Baluchestan, Zahedan, Islamic Republic of Iran

Received: 7 December 2016 / Revised: 14 May 2017 / Accepted: 3 July 2017

Abstract

The present study examined the effect of three methods of preparation on the properties and catalytic performance of Cu-Mn/SiO_2 catalysts for the water gas shift reaction (WGSR). Impregnation and coprecipitation and the new approach of thermal decomposition of $[Cu(H_2O)_6][Mn(dipic)_2].2H_2O/SiO_2$ inorganic precursor complex were used for the synthesis of the silica-supported copper-manganese mixed oxide catalysts. The calcined catalysts and the precursors used for their preparation were characterized by XRD, SEM, BET, TGA, DSC, and FTIR spectroscopy. The WGSR was assessed at 180 to 320 °C. The results showed that thermal decomposition of inorganic precursor complex is more convenient than impregnation and coprecipitation for preparing active and stable Cu-Mn/SiO_2 catalysts for the WGSR.

Keywords: Thermal decomposition; Complex; Bimetallic nanocatalyst; Low-temperature water-gas shift reaction.

Introduction

The solid-catalyzed water gas shift reaction (WGSR), ($CO+H_2O \leftrightarrows CO_2+H_2$), where carbon monoxide and water are converted into hydrogen and carbon dioxide is an important step in many industrial processes [1]. Solid catalysts have been extensively employed in industrial catalytic processes to produce pure hydrogen and reduce CO in H_2-rich reformate or to control the H_2/CO ratio of syngas [2]. WGSR is also useful in fuel cell technology for removing a high percentage of CO by controlling reaction temperatures [3-4].

Its moderate exothermicity (ΔH_{298} = -41.1 $kJmol^{-1}$) means that the WGSR occurs in two distinct stages with the use of catalysts designed specifically for each stage. The initial phase is a conversion at high-temperature (300 to 400 °C) by applying a catalyst of iron-chromium spinel. The second step occurs at a lower temperature (200 to 250 °C) with a highly-active copper-zinc oxide catalyst [5]. Catalysts based on copper are routinely used in industry for hydrogenation, such as in the synthesis of methanol or WGSR at low temperatures.

Copper is commonly called a low-temperature catalyst and it has frequently been used at temperatures below 300 °C because sintering can deactivate catalysts such as copper. The copper-based catalyst for WGSR can be deactivated by H_2O at low temperatures. Cu-based spinel catalysts with highly dispersed Cu have

* Corresponding author: Tel: +985431136331; Fax: +985433446565; Email: ali@hamoon.usb.ac.ir

been evaluated to overcome the low stability of Cu particles. Studies have prepared other base metal catalysts which are superior to conventional Cu-ZnO-Al_2O_3 catalysts. Copper-manganese mixed spinel oxides have shown excellent WGSR activity that is comparable to that of conventional Cu/ZnO/Al_2O_3 catalyst despite their low surface area [1-4]. Further enhancement of the WGSR activity of the Cu-Mn catalyst can be developed using alternative preparation methods that facilitate homogeneous mixing of components.

Studies have prepared Cu/Mn oxide catalysts by coprecipitation [2-6], urea homogeneous coprecipitation [2], sol-gel (organic acid complex) [2], pechini [2], and combustion [7] methods for various catalytic processes.

Thermal decomposition, or thermolysis, is a chemical decomposition of a substance by heating, whereas combustion, or burning, is a high-temperature exothermic redox chemical process between the reductant and an oxidant, usually atmospheric oxygen, that produces oxidized solid and gaseous products.

The use of an inorganic precursor complex is an ideal technique for preparation of materials such as for two (or more) metallic or oxide phases. Its benefits include excellent metal interaction, even dispersion of two (or more) metals in every part of the support, and maximum loading to enhance catalytic performance [8-12].

Porous materials have attracted considerable attention as catalysts, adsorbents, and chemical supports. Inorganic porous materials are desirable supports for heterogeneous catalysts because they offer high thermal and chemical stability. Porous silica possesses all the properties of inorganic materials and offers a large specific surface area, a well-defined pore size that is tunable, adjustable hydrophobic or hydrophilic properties, suitable opportunities for good immobilization, and excellent loading and dispersion of catalytic species [13].

A detailed study on a water gas shift reaction (WGSR) active Cu-Mn/SiO_2 catalytic system is presented in the present work. The main objective of this work is the investigation of the effects of the preparation method on the structural properties and catalytic activity of Cu-Mn/SiO_2 catalysts in WGSR. The corresbonding results of the Cu-Mn/SiO_2 catalyst prepared using the thermal decomposition of silica-supported $[Cu(H_2O)_6][Mn(dipic)_2].2H_2O$, a supported inorganic precursor complex, is also addressed. A comparative study of the physicochemical characteristics of the catalysts was carried out using X-ray diffraction (XRD), scanning electron microscopy (SEM), the Brunauer-Emmett-Teller (BET) method, thermal gravimetric analysis (TGA), and differential scanning calorimetry (DSC).

Materials and Methods

Materials

Reagent-grade $Mn(NO_3)_2.4H_2O$, $Cu(NO_3)_2.3H_2O$, SiO_2, and pyridine-2,6-dicarboxylic acid (dipicolinic acid, H_2dipic) were obtained from Aldrich and used as received. Ammonium pyridine-2,6-dicarboxylate (ammonium dipicolinate, $(NH_4)_2$dipic) was prepared as suggested in the literature using the interaction of ammonia (15 ml) and pyridine-2,6-dicarboxylic acid (1000 mg; 6 mmol) at 75 °C. The SiO_2 used was amorphous nanoparticle and had a specific surface area of 200 m^2/g, an average pore diameter of 18-22 nm, and an average pore volume of 1.4-2 cm^3/g.

Preparation of catalysts

Preparation of $[Cu(H_2O)_6][Mn(dipic)_2].2H_2O$

Ammonium pyridine-2,6-dicarboxylate (402 mg; 2 mmol) was dissolved in water (20 ml) and added dropwise under continuous stirring to an aqueous solution (5 ml) of $Mn(NO_3)_2.4H_2O$ (251 mg; 1 mmol). After 4 h of stirring at room temperature, $Cu(NO_3)_2.3H_2O$ (242 mg; 1 mmol) was added to the solution. The mixture was blended for 1 h to react and subsequently left in the air at room temperature. After three weeks, a yield of about 60% water-soluble light blue crystals was achieved. Anal. Calc. for $C_{14}H_{22}CuMnN_2O_{16}$ (592800 mg): C, 28.36; H, 3.74; N, 4.72. Found: C, 27.98; H, 3.66; N, 4.61%. IR (KBr, cm^{-1}): 3421, 3200, 1635, 1621, 1596, 1509, 1437, 1382, 1350, 1274, 1182, 1087, 768, 737, 687, 592, 445, 419. UV-Vis (H_2O, nm): 216, 271, 760. Λ_M (H_2O) =145 ohm^{-1} cm^2 mol^{-1}.

Preparation of $[Cu(H_2O)_6][Mn(dipic)_2].2H_2O/SiO_2$ precursor

$[Cu(H_2O)_6][Mn(dipic)_2].2H_2O$ (10 mmol; 5930 mg) was dissolved in 100 ml of distilled water and then added to SiO_2 (600 mg). The suspension was mixed and vaporized to dehydration at 30 °C.

Preparation of silica-supported copper-manganese catalyst, Cu-Mn/SiO_2

The final calcined catalyst was produced as follows: $[Cu(H_2O)_6][Mn(dipic)_2].2H_2O/SiO_2$ precursor was calcined at 600 °C for 4 h in an atmosphere of static air in an electric furnace. The final grey Cu-Mn/SiO_2 catalyst was produced and retained in a desiccator. This sample was labeled as CuMnSiIPC.

Preparation of reference catalysts

Cu-Mn/SiO_2 reference catalysts were produced by impregnation and coprecipitation for comparison. In coprecipitation, aqueous solutions of manganese nitrate ($Mn(NO_3)_2.4H_2O$) and copper nitrate ($Cu(NO_3)_2.3H_2O$) (1:1) were mixed with the required quantity of silica and Na_2CO_3 at 30 °C. The pH was kept constant by adding an aqueous solution of NaOH dropwise. The precipitate was then aged for 6 h. After aging, the suspension was filtered and the precipitate was washed. The precipitate was dried at 120 °C and then calcined at 600 °C for 4 h.

In the impregnation method, manganese nitrate and copper nitrate were dissolved in water and impregnated into the silica support. The suspension was aged for 6 h at 30 °C and then filtered. The precipitate was then dried overnight at 120 °C. The precursor was then calcined at 600°C for 4 h. These samples are labeled as CuMnSiCP (coprecipitation) and CuMnSiIM (impregnation).

Catalyst characterization

XRD

Powder XRD was carried out using a FK60-04 diffractometer. The scans were performed using a 2θ step size of 0.02° and a counting time of 1.0 s using a CuKα radiation source generated at 40 kV and 30 mA. Data was collected over a 2θ range of 5° to 90°. The phases were identified by matching experimental patterns to a database provided by the International Centre for Diffraction Data (file PDF2).

SEM

The morphology of the catalysts and their precursors was observed by means of a Jeol JSM 5410 scanning electron microscope operating at 10 kV.

BET measurement of surface area

Measurement of the surface area and pore volume of the catalyst precursors and calcined specimens using the BET method were carried out by N_2 physisorption using a Quantachrome Nova 4200 apparatus. Each catalyst sample was degassed under nitrogen atmosphere at 300°C for 3 h. The BET surface areas and pore volumes were obtained by evacuating the samples at -196 °C for 66 min.

TGA

Measurement of weight change in the catalyst precursor was done by using a TGA-PL (England) under a flow of dry air. The room temperature was increased to 600 °C using a linear programmer at increments of 10°C/min. The sample weight was 15 and 20 mg.

DSC

DSC was carried out on a DSC 200 F3 (Netzsch) under a flow of dry air using a linear programmer at increments of 10 °C/min.

Elemental analysis, conductometry, FTIR, UV-vis, and spectroscopy atomic absorption

Elemental analysis was performed using a Perkin-Elmer 2400 CHNS/O elemental analyzer. Conductometry was carried using a Ciba-Corning checkmate 90 conductometer. FTIR spectra were recorded as KBr pellets on a FT-IR Jasco 460 spectrophotometer. UV–vis spectra were obtained using a JASCO 7850 spectrophotometer. Spectroscopy of metals based on atomic absorption was carried out using a Varian AA50.

Catalytic activity measurement

WGSR activity measurement was performed in a fixed bed micro-reactor under atmospheric pressure. Before the catalytic runs, the catalysts (1000 mg) were subjected to reduction *in situ* at atmospheric pressure under a flowing H_2-N_2 stream (N_2/H_2 = 1; flow rate of each gas = 30 ml min^{-1}) at 400 °C for 6 h. Afterwards, the H_2O/CO (4:1) mixture with a GHSV of 3600 h^{-1} was used instead of the N_2/H_2. WGSR activity was measured at 180 to 320°C for 8 h at each temperature. Analysis of the reactor inlet and outlet gases was carried out online by means of a gas chromatograph (Varian, Model 3400 series). Conversion of CO and selectivity of CO_2 were applied for the evaluation of catalyst activity as:

CO conversion (%)={[(moles of CO_{in}) – (moles of CO_{out})] / moles of CO_{in}} × 100

CO_2 selectivity (%)=[moles of CO_2 / moles of products] × 100

Results and Discussion

Complex characterization

The reaction of the molecular ions $[Mn(dipic)_2]^{2-}$ with complementary unit $[Cu(H_2O)_6]^{2+}$ at room temperature (298 K) led to formation of the heterodinuclear hexaaqua dipicolinate complex $[Cu(H_2O)_6][Mn(dipic)_2]$. The details of the consecutive reactions are condensed in Eqs.(1) and (2) as:

$Mn(NO_3)_2.4H_2O + 2(NH_4)_2dipic \rightarrow (NH_4)_2[Mn(dipic)_2] + 2NH_4NO_3 + 4H_2O$ (1)

$(NH_4)_2[Mn(dipic)_2]+[Cu(H_2O)_6](NO_3)_2 \rightarrow [Cu(H_2O)_6]$

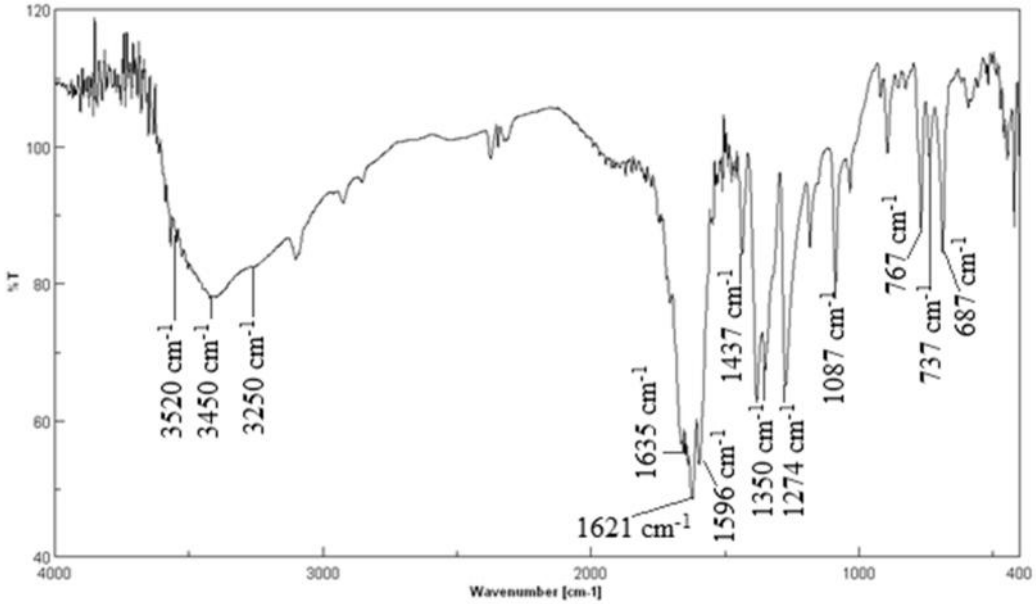

Figure 1. FT-IR spectrum of $[Cu(H_2O)_6][Mn(dipic)_2].2H_2O$

$[Mn(dipic)_2]+2NH_4NO_3$ (2)

In the suggested structure of the heterodinuclear complex $[Cu(H_2O)_6][Mn(dipic)_2].2H_2O$, the divalent anion $[Mn(dipic)_2]^{-2}$ is produced from the coordination of two dipicolinate ligands acting as tridentate ligands through their carboxylic oxygen atoms and the nitrogen atoms to the Mn(II) ion for which the charge is balanced by the $[Cu(H_2O)_6]^{2+}$ divalent cation. The infrared spectrum of the $[Cu(H_2O)_6][Mn(dipic)_2].2H_2O$ complex (Fig. 1) shows two sets of vibrations for the aqua and dipicolinate ligands. The $\nu(H_2O)$ vibrations correlate with both coordination and free water molecules can be observed to be very strong and broad bands in the 3700-2700 cm^{-1} region, typically with two maxima at about 3520-3450 and 3250-3200 cm^{-1}. Their broadening and shifting to lower energy at about 2700 cm^{-1} and their extremes are representative of intensive H-bonding.

The sharp band at 1635 cm^{-1} can be ascribed to crystallization of water molecules in the crystal lattice [14]. Within the complex IR spectrum, the ν(O-H) vibrations associated with the carboxylate group in the dipicolinate ligands are absent, confirming deprotonation of the –COOH group and coordination to the metal [15]. Two intense IR bands related to asymmetric $\nu_{as}(COO)$ and symmetric $\nu_s(COO)$ are stretching vibrations of the dipicolinate carboxylate groups for the complex at 1621 and 1437 cm^{-1}, respectively. They shifted after formation of the complex than free dipicolinate ligand. The frequency differences between the asymmetric and symmetric stretches of the dipicolinate carboxylate groups ($\Delta\nu(COO)$ = 184 cm^{-1}) suggest a monodentate mode of carboxylate moiety binding to the Mn(II) ions [15-17]. The δ(COO) mode is evident in the spectrum of the free dipicolinate ligand as a high-intensity band at 701 cm^{-1}; in the complex, this strong band has shifted to 737 cm^{-1}.

Three high or medium intensity bands associated with the ν(C-O) vibrations of the dipicolinate carboxylate groups can be observed at 1087, 1274, and 1350 cm^{-1} [16,18-19]. The strong absorption band at 1596 cm^{-1} is from the ν(C=C) + ν(C=N) vibration of the pyridine ring in the dipicolinate ligand. Ring wagging vibrations of the pyridine groups can be observed at 687 and 767 cm^{-1} [15].

Atomic absorption spectroscopy provides adequate values for Cu(II) and Mn(II) ions in the complex, verifying the presence in equimolar amounts of those metals. Analysis of the UV/vis spectrum of the complex allows allocation of copper to the cationic and manganese to the anionic part of the compound.

Electronic excitation of the $[Cu(H_2O)_6][Mn(dipic)_2].2H_2O$ complex in a water solution reveals several absorption bands in the UV and visible regions (Fig. 2). In the visible region, the broad, intense band at 760 nm can be ascribed to d–d transitions of the Cu(II) hexa aqua species and suggests that Mn(II) binds to the dipicolinate ligand and Cu(II) forms a hexaaqua cationic moiety [20]. Two intensive absorption bands at 216 and 271 nm in the UV region can be attributed to intra-ligand $\pi \rightarrow \pi^*$ transitions of the dipicolinate ligand [16].

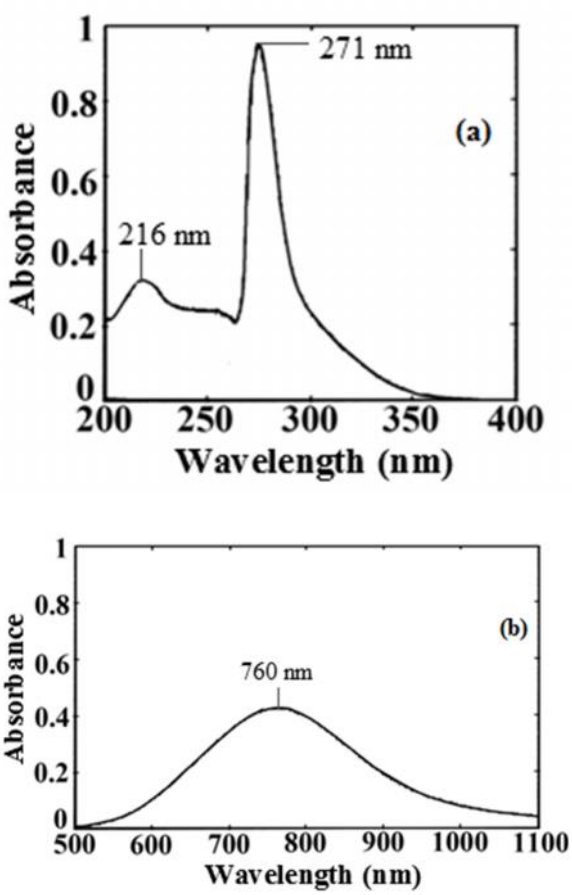

Figure 2. UV (a) and visible (b) regions of electronic spectra of $[Cu(H_2O)_6][Mn(dipic)_2].2H_2O$

Measurement of the molar conductivity at infinite dilution of the $[Cu(H_2O)_6][Mn(dipic)_2].2H_2O$ complex (Λ_M (H_2O) = 145 ohm^{-1} cm^2 mol^{-1}) indicates that the compound is a 1:1 electrolyte in water. This provides structural information and corroborates the existence of the cationic $[Cu(H_2O)_6]^{2+}$ and anionic $[Mn(dipic)_2]^{-2}$ components in the aqueous solution of this complex [21].

Characterization of catalyst and its precursor

The FTIR spectrum of the calcined catalyst (Fig. 3) demonstrates the characteristic bands of absorption for pure silica. The asymmetric and symmetric stretching vibrations of the Si-O-Si network can be observed to be a very strong band at 1105 cm^{-1} with a shoulder at 1200 cm^{-1} and a weak IR absorption band at 818 cm^{-1}. The bending mode of -OSi-O- and bending vibration of Si-O bonds can be observed as an intense band at 460 cm^{-1} and a medium intensity absorption band at 595 cm^{-1}, respectively. The OH stretching and H-OH bending vibrations of physically-adsorbed water are evident as broad bands at 3421 and 1635 cm^{-1}, respectively [9]. In the IR spectra of the pure silica and the calcined catalyst, the typical Si-O-Si vibrations are equivalent, which suggests that the metal oxides in the calcined catalyst do not notably influence the Si-O-Si vibrations. As a consequence of inter-atomic vibration, the characteristic absorption bands of the metal oxides normally appear below 1000 cm^{-1} [22]. The Mn-O and Cu-O stretching vibrations associated with crystalline CuO and $Cu_xMn_{3-x}O_4$ in the calcined catalyst are well-defined bands at 678 and 534 cm^{-1}, respectively [23].

The XRD pattern for the precursor is shown in Fig. 4. As expected for a well-crystallized specimen, the diffraction lines with high intensities and low half-

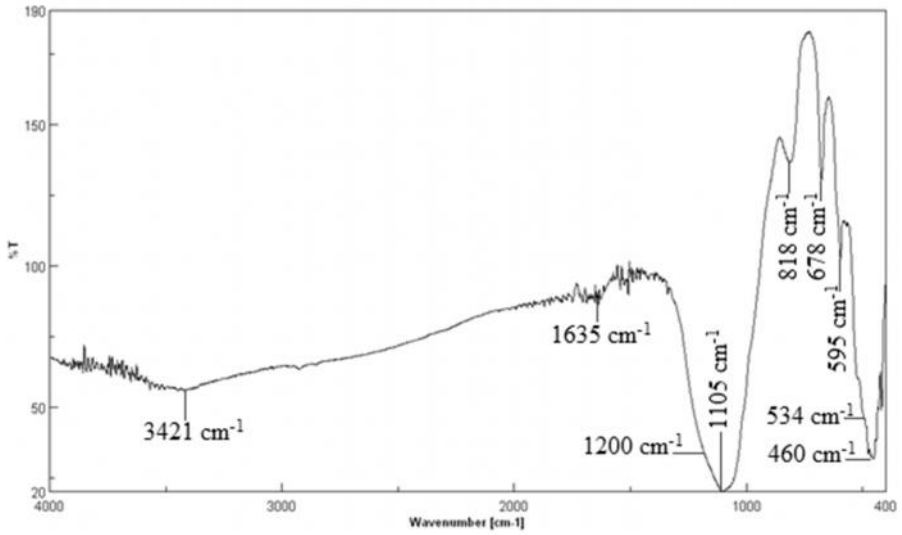

Figure 3. FT-IR spectrum of Cu-Mn/SiO_2 catalyst calcined at 873 K

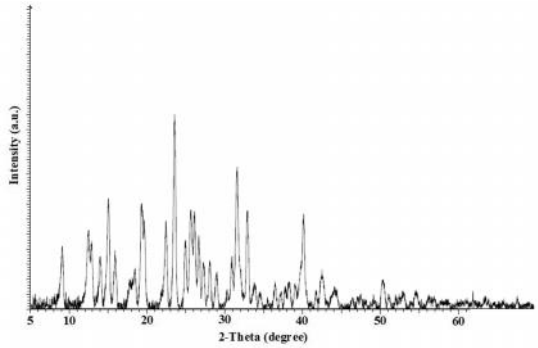

Figure 4. Powder X-ray diffraction pattern of $[Cu(H_2O)_6][Mn(dipic)_2].2H_2O/SiO_2$ precursor

widths are observed in the precursor XRD pattern (at 2θ = 9.02°, 12.4°, 12.8°, 13.9°, 15.07°, 19.3°, 22.4°, 23.5°, 24.9°, 25.6°, 26.1°, 31.6°, 32.9° and 40.1°). Figure 5 shows the XRD pattern of the calcined CuMnSiIPC catalyst prepared from a novel precursor. The XRD patterns of the calcined CuMnSiIM and CuMnSiCP catalysts from impregnation and coprecipitation serve as references in Fig. 5. All samples exhibit the characteristic diffraction peaks of CuO (JCPDS 01-1117), $CuMn_2O_4$ (JCPDS 11-0480), $Cu_{1.2}Mn_{1.8}O_4$ (JCPDS 35-1029), $Cu_{1.4}Mn_{1.6}O_4$ (JCPDS 35-1030), and SiO_2 (JCPDS 02-0278).

No detectable reflections of silicates can be distinguished in the XRD patterns of calcined catalysts. This feature is most probably evidence of the lack of obvious interaction between the Cu-Mn catalysts and the SiO_2 support. The average sizes of the CuO and $Cu_xMn_{3-x}O_4$ crystallites on calcined CuMnSiIPC, CuMnSiIM, and calcined CuMnSiCP reference catalysts were calculated by applying Scherrer's equation to CuO (111) and $Cu_xMn_{3-x}O_4$ (311) crystallographic planes (Table 1).

The results indicate that thermal decomposition of the inorganic precursor complex enhanced dispersion of CuO and $Cu_xMn_{3-x}O_4$ and facilitated the formation of smaller particles than those existing on the CuMnSiIM and CuMnSiCP samples. XRD analysis of the reduced Cu-Mn/SiO_2 catalyst (Fig. 6) revealed that the CuO and $Cu_xMn_{3-x}O_4$ phases decomposed and caused the coexistence of MnO (JCPDS 01-1206) and Cu_2O (JCPDS 34-1354) phases.

To evaluate the thermal stability of $[Cu(H_2O)_6][Mn(dipic)_2].2H_2O$ complex, TGA was carried out on $[Cu(H_2O)_6][Mn(dipic)_2].2H_2O/SiO_2$ precursor at 30 to 600 °C in increments of less than 10°C/min^{-1} (Fig. 7a). The thermal decomposition of the precursor occurred in three steps of weight loss. As the temperature increased, the first and second degradation

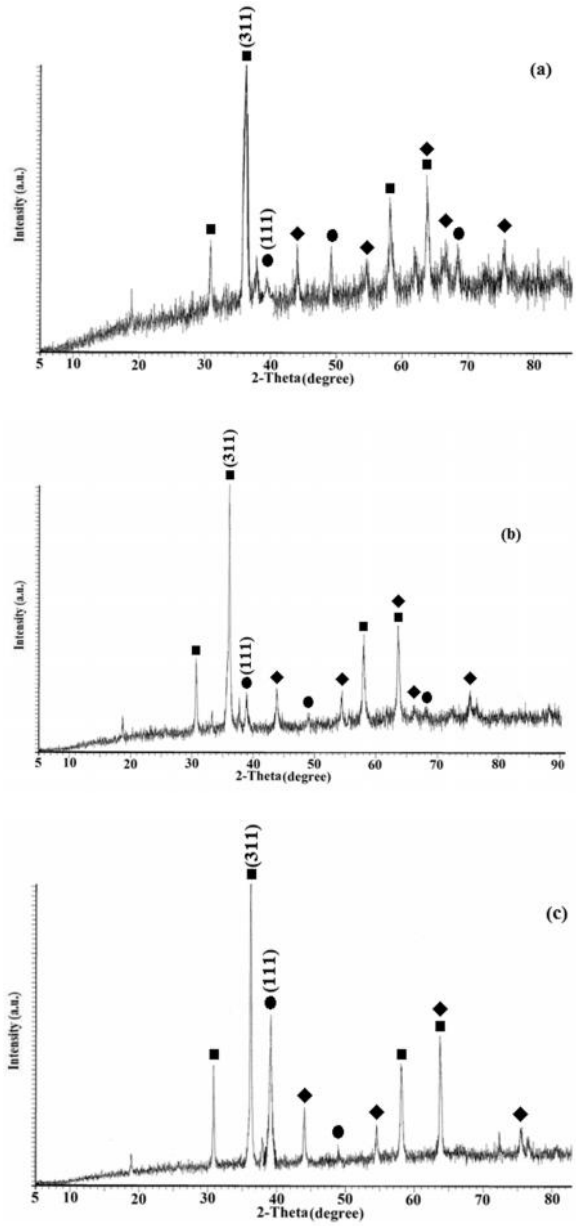

Figure 5. Powder X-ray diffraction patterns of (a) calcined CuMnSiIPC catalyst and calcined reference catalysts prepared by (b) impregnation, and (c) co-precipitation: ● - CuO (JCPDS 01-1117); ■ - $CuMn_2O_4$ (JCPDS 11-0480); ■ - $Cu_{1.2}Mn_{1.8}O_4$ (JCPDS 35-1029); ■ - $Cu_{1.4}Mn_{1.6}O_4$ (JCPDS 35-1030); ◆ - SiO_2 (JCPDS 02-0278).

steps occurred at 80 to 270 °C and can be attributed to the elimination of two lattice and six coordinated water molecules, respectively. The aquated species is stable up to 290°C, but upon further heating, another step of weight loss occurs that continued to 600°C. This step of

Table 1. Textural properties and structural parameters of Cu-Mn catalysts prepared using different methods

Sample	BET surface area (m^2/g)	Pore volume (cm^3/g)	d_{CuO} (nm)	$d_{CuxMn3-xO4}$ (nm)
$[Cu(H_2O)_6][Mn(dipic)_2].2H_2O/SiO_2$	0.98	0.07		
CuMnSiIPC catalyst	101.3	1.26	16.02	15.78
Reference catalyst (imp)	86.4	0.82	32.04	31.78
Reference catalyst (cop)	79.6	0.53	32.1	31.86

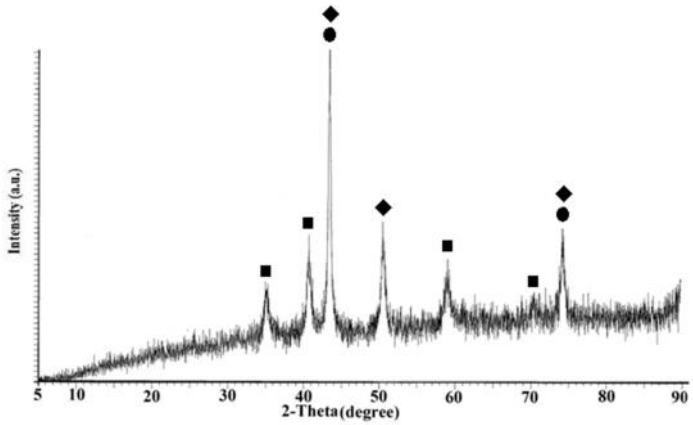

Figure 6. Powder X-ray diffraction pattern of reduced CuMnSiIPC catalyst: ●- Cu_2O (JCPDS 34-1354); ■- MnO (JCPDS 01-1206); ◆- SiO_2 (JCPDS 02-0278).

weight change can be attributed to the decomposition of the coordinated dipicolinate ligands. The stable oxide phases recognized using FTIR spectroscopy and XRD have been generated as the final decomposition products.

Thermal decomposition of reference sample CuMnSiIM prepared by impregnation required four steps of weight loss (Fig. 7b). As the temperature increased, the first and second decomposition steps occurred at 80 to 240 °C and can be attributed to the elimination of physically-adsorbed water and deaquation from the micropores of the hydroxide gel, respectively. The last two steps of weight loss at 250 to 550 °C can be attributed to nitrate decomposition and the pursuant dehydroxylation.

Three main thermal effects can be observed in the TGA profile of reference sample CuMnSiCP prepared by coprecipitation (Fig. 7c). As the temperature increased, the first decomposition step at 80 to 170 °C can be attributed to the removal of absorbed water. The second and third steps of weight loss occur at 180 to 550 °C and can be attributed to the decomposition of hydroxy (basic nitrate precursors) and the subsequent decomposition of hydroxyl (basic carbonate precursors).

DSC supplied supplemental corroboration for the existence of the diverse components and appraisal of their thermal behavior. As shown for the $[Cu(H_2O)_6][Mn(dipic)_2].2H_2O/SiO_2$ precursor in Fig. 8a, the endothermic peaks at 80 to 140 °C represent the elimination of water molecules from the catalyst precursor and the three exothermic peaks at 180 to 300 °C can be attributed to the degradation of dipicolinate ligands. The two exothermic peaks at 300 to 580 °C can be attributed to the generation of stable CuO and $Cu_xMn_{3-x}O_4$ oxide phases, which were confirmed by FTIR spectroscopy and XRD as the final decomposition products [24].

DSC analysis was carried out on reference sample CuMnSiIM prepared by impregnation. Fig, 8b shows one endothermic peak at 60 to 120 °C that is representative of the elimination of physically-adsorbed water from the material and three exothermic peaks at 220 to 520 °C that can be attributed to the generation of the stable oxide phases.

For comparison, DSC measurement was carried out on reference sample CuMnSiCP prepared by coprecipitation. As shown in Fig. 8c, two endothermic peaks at 60 to 240 °C can be attributed to the elimination of physically-adsorbed and chemically-bound water molecules and the two exothermic peaks at 280 to 480 °C can be attributed to the generation of stable oxide phases.

These investigations indicate that the precursors were subject to morphological reactions and phase changes, but the measurement techniques were not

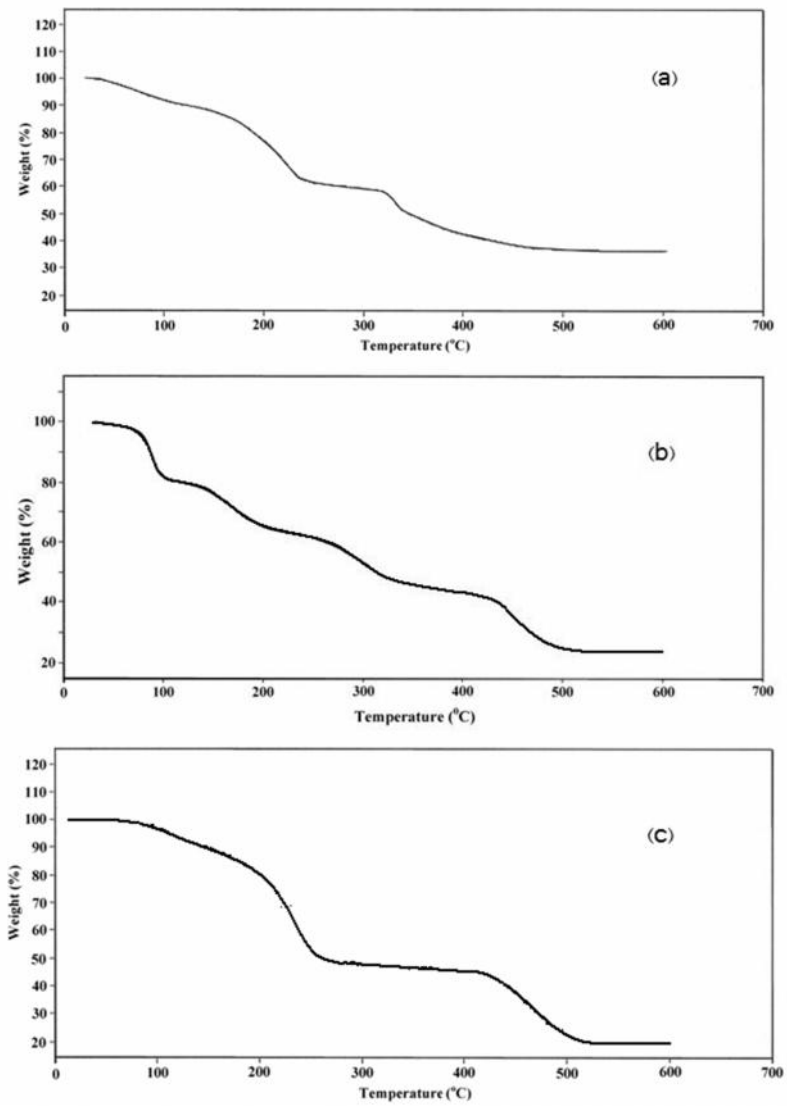

Figure 7. Thermograms of (a) $[Cu(H_2O)_6][Mn(dipic)_2].2H_2O/SiO_2$ precursor and reference samples prepared by (b) impregnation, and (c) co-precipitation before calcinations

sufficiently sensitive to reveal all details of these changes. The precursor and calcined catalysts were then characterized by means of SEM (Fig. 9). The SEM results show that the precursor and calcined samples have different morphologies and textures. The SEM image of the catalyst precursor showed various agglomerations of crystalline-shaped particles of different sizes (Fig. 9a). These results are in good agreement with the XRD findings. Calcination at less than 600 °C for 4 h in an atmosphere of static air resulted in morphological changes in the calcined catalysts. The calcined CuMnSiIPC catalyst exhibited agglomerate sizes that were smaller than those of the catalyst precursor (Fig. 9b). The morphological properties of the calcined reference samples CuMnSiIM and CuMnSiCP were different from the calcined CuMnSiIPC catalyst. These calcined reference catalysts are composed of larger particles than those in the calcined CuMnSiIPC catalyst (Figs. 9c and 9d).

Identification of the catalyst precursor and all calcined catalysts was performed by BET measurement and the results are presented in Table 1. As shown, the catalyst precursor had a much lower BET specific surface area and pore volume (0.98 m^2/g and 0.07 cm^3/g, respectively) than the calcined CuMnSiIPC catalyst (101.3 m^2/g and 1.26 cm^3/g, respectively). It is apparent that the process of calcination changed the surface areas and pore volumes of the samples. A suitable preparation method (thermal decomposition of $[Cu(H_2O)_6][Mn(dipic)_2].2H_2O/SiO_2$ inorganic precursor

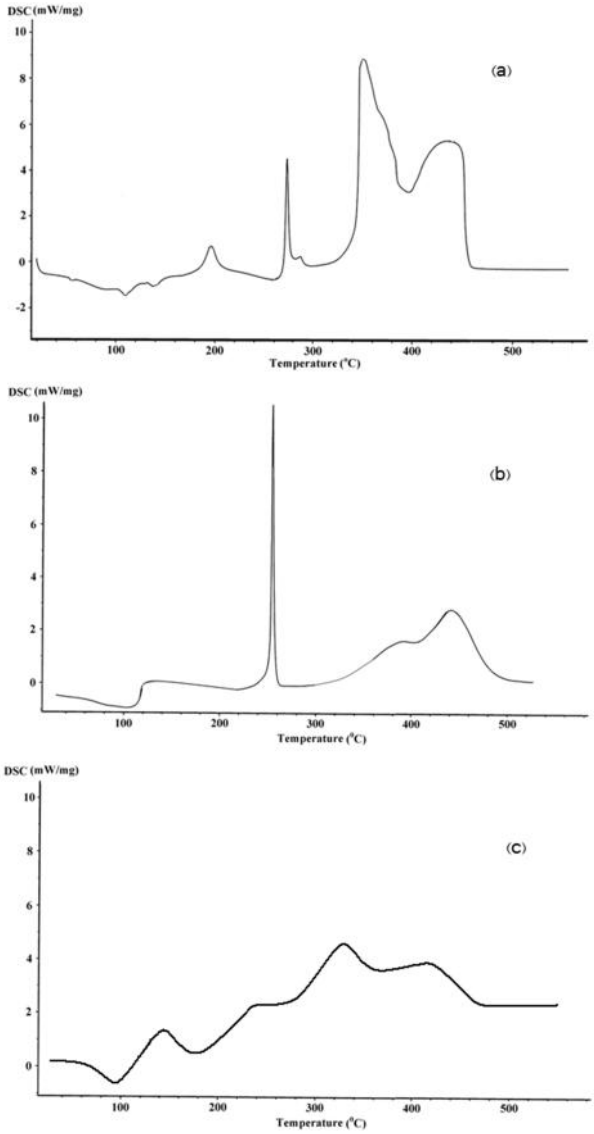

Figure 8. DSC curves for (a) $[Cu(H_2O)_6][Mn(dipic)_2].2H_2O/SiO_2$ precursor and reference samples prepared by (b) impregnation, and (c) co-precipitation before calcinations

complex) and the choice of silica as a support increased the BET specific surface area and pore volume of the calcined CuMnSiIPC catalyst [25]. The BET data for all calcined catalysts and catalyst precursors are in excellent agreement with the SEM findings. The finer particles in the calcined catalysts would be expected to have higher BET specific surface areas and pore volumes than the catalyst precursor. The results also showed that the calcined CuMnSiIPC catalyst has a higher BET specific surface area and pore volume than calcined reference samples CuMnSiIM and CuMnSiCP and several Cu/Mn oxide catalysts from earlier studies [2-4]. This is convincing evidence for the improvement in a dispersion of the active oxide phases and the enhancement of catalytic performance of this calcined CuMnSiIPC catalyst.

WGSR activity measurements

Effect of temperature

The experiments for WGSR activity measurement were repeated three consecutive times. Fig. 10 shows the temperature dependence of CO conversion for calcined Cu-Mn/SiO_2 oxide catalysts prepared by impregnation, coprecipitation, and thermal decomposition of inorganic precursor complex along with the Cu and Mn catalysts for low-temperature WGSR at 180 to 320 °C. The values associated with the influence of reaction temperature on WGSR activity of

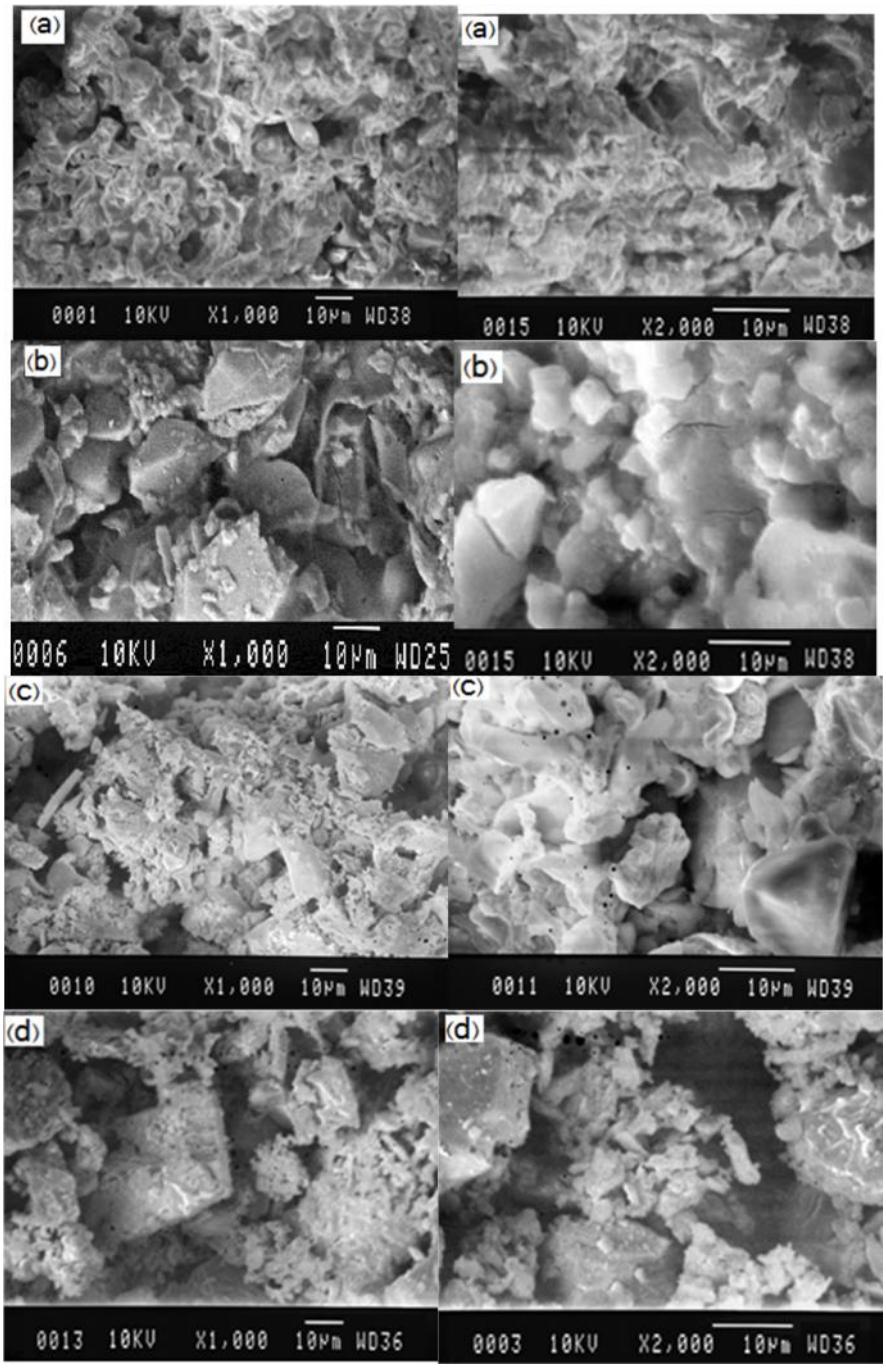

Figure 9. SEM micrographs of: (a) $[Cu(H_2O)_6][Mn(dipic)_2].2H_2O/SiO_2$ precursor, (b) calcined CuMnSiIPC catalyst and calcined reference catalysts prepared by (c) impregnation, and (d) co-precipitation

the calcined CuMnSiIPC catalyst in terms of CO conversion and also CO_2 and methane selectivity are reported by at least three determinations, and results are presented in Table 2.

The WGSR activity of the calcined CuMnSiIPC catalyst increased as temperature increased from 180 to 220 °C and 78.4% CO conversion was achieved at 220°C and decreased as the temperature increased from 220 to 320 °C and 61.2% CO conversion was achieved at 320 °C. In view of the temperate exothermicity of the WGSR according to Le Chatelier's principle, an increase in temperature decreased the conversion of CO and selectivity of CO_2. An increase in temperature in WGSR shifts equilibrium to the reverse reaction that

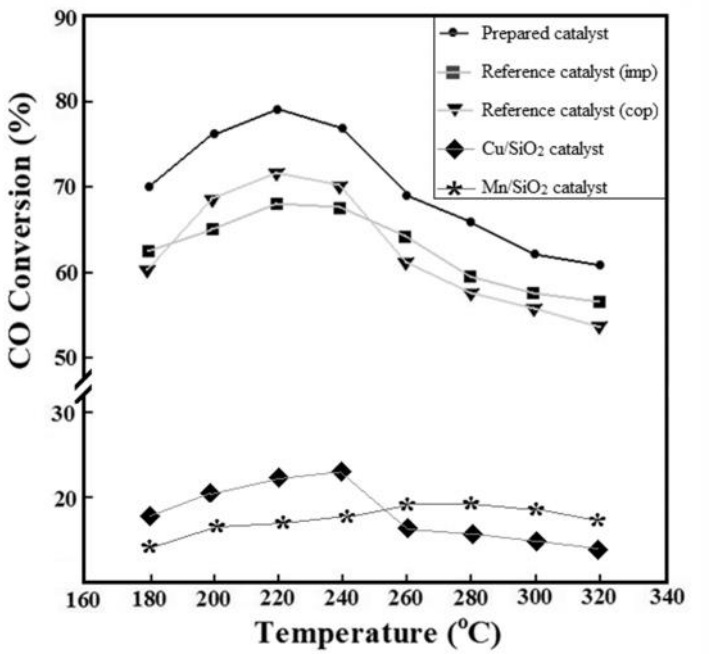

Figure 10. Effect of reaction temperature on CO Conversion of CuMnSiIPC and reference CuMnSiIM and CuMnSiCP catalysts in the water gas shift reaction

Table 2. Influence of reaction temperature on catalytic performance of the CuMnSiIPC catalyst in the water gas shift (WGS) reaction

Temperature (°C)	CO conversion (%)				CO_2 selectivity (%)				CH_4 selectivity (%)			
	#1	#2	#3	Mean	#1	#2	#3	Mean	#1	#2	#3	Mean
180	68.2	71.6	70.8	70.2	98.2	99.1	98.5	98.6	1.8	0.9	1.5	1.4
200	75.1	76.3	78.7	76.7	97.6	98.1	99.2	98.3	2.4	1.9	0.8	1.7
220	78.1	79.5	77.6	78.4	96.3	97.2	96.0	96.5	3.7	2.8	4.0	3.5
240	77.9	77.6	77.0	77.5	95.6	95.5	94.8	95.3	4.4	4.5	5.2	4.7
260	67.3	68.8	69.1	68.4	91.4	92.0	92.3	91.9	8.6	8.0	7.7	8.1
280	64.2	63.8	66.7	64.9	90.3	90.1	91.1	90.5	9.7	9.9	8.9	9.5
300	63.1	62.8	61.3	62.4	90.2	90.0	89.5	89.9	9.8	10.0	10.5	10.1
320	61.5	62.9	59.2	61.2	90.1	90.2	89.1	89.8	9.9	9.8	10.9	10.2

H_2O/CO molar ratio: 4, GHSV: 3600 h^{-1}, 1.0 g of catalyst.

can also generate by-products such as methane by methanation [26].

The CuMnSiIPC sample exhibited considerably higher catalytic activity than that observed for reference samples CuMnSiIM and CuMnSiCP and the Cu and Mn catalysts. The calcined CuMnSiIPC catalyst achieved 78.4% CO conversion at 220 °C.

The preparation method of the catalyst influences its catalytic activity and behavior. A decrease in crystallite size increased the BET specific surface area and improved the catalytic function of calcined CuMnSiIPC catalyst compared with the CuMnSiIM and CuMnSiCP reference catalysts. This difference relates to the exclusive features of the preparation method used. Thermal degradation of inorganic precursor complexes is advantageous for controlling the size and bimetallic composition, consequently, most nanoparticle yields maintain the original bimetallic properties of the inorganic precursor complex composition. This clearly demonstrates the effectiveness of inorganic complexes as catalyst precursors.

Stability test

Another benefit of the calcined CuMnSiIPC catalyst was its stability. Measurement of catalytic stability was conducted on all catalysts calcined at 220 °C, the temperature at which these catalysts achieved maximum CO conversion. The profile of CO conversion versus time for these catalysts is shown in Fig. 11. The WGSR activity of all calcined catalysts was stable within the 8 h test time. CO conversion of the calcined CuMnSiIPC catalyst decreased by 2.7% over the 24 h of testing.

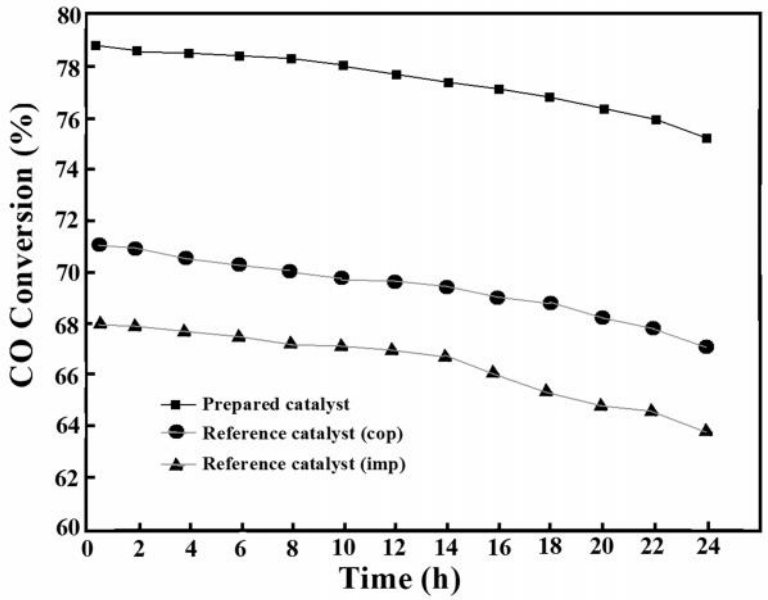

Figure 11. Stability performances of Cu-Mn/SiO_2 catalysts prepared using different methods at 220°C.

Conclusion

Application of thermal decomposition of inorganic precursor complex, coprecipitation, and impregnation resulted in catalysts such as Cu-Mn/SiO_2 oxide with distinct structural features. Analyze of the physico-chemical properties of the $[Cu(H_2O)_6][Mn(dipic)_2].2H_2O$ complex, precursors, and calcined catalysts using XRD, SEM, BET, TGA, DSC, and FTIR spectroscopy certified that calcination generates solid copper and manganese oxides and gaseous carbon and nitrogen oxides. Evaluation of the catalytic performance of WGSR at low temperatures revealed that thermal decomposition of $[Cu(H_2O)_6][Mn(dipic)_2].2H_2O/SiO_2$ precursor is a more appropriate route for the preparation of active and stable copper-manganese oxide catalysts. This method is a promising alternative to the preparation of highly-dispersed supported dual catalysts for application in catalytic processes. Catalytic measurements at 180 to 320 °C confirmed the superior performance of the CuMnSiIPC catalyst compared with the reference CuMnSiIM and CuMnSiCP catalysts. It is suggested that the higher activity of this sample relates to the smaller particle sizes and higher BET specific surface areas in comparison with other copper-manganese catalysts [2-5].

The effect of a range of operation variables such as space velocity, H_2O/CO molar feed gas ratio and pressure on the performance of this catalyst can be investigated and completed in future.

Acknowledgement

The authors are grateful to the University of Sistan and Baluchestan (USB) for financial support.

References

1. Ratnasamy C. and Wagner J.P. Water gas shift catalysis. *Catal. Rev.* **51**: 325-440 (2009).
2. Tanaka Y., Takeguchi T., Kikuchi R. and Eguchi K. Influence of preparation method and additive for Cu-Mn spinel oxide catalyst on water gas shift reaction of reformed fuels. *Appl. Catal. A.* **279**: 59-66 (2005).
3. Tanaka Y., Utaka T., Kikuchi R., Takeguchi T., Sasaki K. and Eguchi K. Water Gas Shift Reaction for the Reformed Fuels over Cu/MnO Catalyst Prepared via Spinel-Type Oxide. *J. Catal.* **215**: 271–278 (2003).
4. Tanaka Y., Utaka T., Kikuchi R., Sasaki K. and Eguchi K. Water gas shift reaction over Cu-based mixed oxides for CO removal from the reformed fuels. *Appl. Catal. A.* **242**: 287-295 (2003).
5. Hutchings G.J., Copperthwaite R.G., Gottschalk F.M., Hunter R., Mellor J., Orchard S.W. and Sangiorgio T. A comparative evaluation of cobalt chromium oxide, cobalt manganese oxide and copper manganese oxide as catalysts for the water-gas shift reaction. *J. Catal.* **137**: 408–422 (1992).
6. Ke-duan Z., Quan-sheng L., Ya-gang Z., Shuang H. and Run-xia H. Effect of precipitator on the texture and activity of copper-manganese mixed oxide catalysts for the water gas shift reaction. *J. Fuel Chem. Technol.* **38**: 445−451 (2010).
7. Papavasiliou J., Avgouropoulos G. and Ioannides T. Steady-state isotopic transient kinetic analysis of steam reforming

of methanol over Cu-based catalysts. *Appl. Catal. B.* **88**: 490-496 (2009).
8. Farzanfar J. and Rezvani A.R. Study of a Mn–Cr/TiO2 mixed oxide nanocatalyst prepared via an inorganic precursor complex for high-temperature water–gas shift reaction. *C. R. Chimie.* **18**: 178-186 (2015).
9. Farzanfar J. and Rezvani A.R. Inorganic complex precursor route for preparation of high-temperature Fischer–Tropsch synthesis Ni–Co nanocatalysts. *Res. Chem. Intermed.* **41**: 8975-9001 (2015).
10. Huang Q., Yan X., Li B., Xu X., Chen Y., Zhu S. and Shen S. Activity and stability of Pd/MMnO*x* (M = Co, Ni, Fe and Cu) supported on cordierite as CO oxidation catalysts. *J. IND. ENG. CHEM.* **19**: 438–443 (2013).
11. Yan X., Huang Q., Li B., Xu X., Chen Y., Zhu S. and Shen S. Catalytic performance of $LaCo_{0.5}M_{0.5}O_3$ (M = Mn, Cr, Fe, Ni, Cu) perovskite-type oxides and $LaCo_{0.5}Mn_{0.5}O_3$ supported on cordierite for CO oxidation. *J. IND. ENG. CHEM.* **19**: 561–565 (2013).
12. Mansouri M., Atashi H., Tabrizi F.F., Mirzaei A.A. and Mansouri G. Kinetics studies of nano-structured cobalt–manganese oxide catalysts in Fischer–Tropsch synthesis. *J. IND. ENG. CHEM.* **19**: 1177–1183 (2013).
13. Ma X., Sun H., Sun Q., Feng X., Guo H., Fan B., Zhao S., He X. and Lv L. Catalytic oxidation of CO and *o*-DCB over CuO/CeO_2 catalysts supported on hierarchically porous silica. *Catal. Commun.***12**: 426–430 (2011).
14. Tabatabaee M., Kukovec B.M. and Kazeroonizadeh M. A unique example of a co-crystal of $[Ag(atr)_2][Cr(dipic)_2]$ (dipic = dipicolinate; atr = 3-amino-1H-1,2,4-triazole) and dinuclear $[Cr(H_2O)(dipic)(\mu\text{-}OH)]_2$, with different coordination environment of Cr(III) ions. *Polyhedron* **30**: 1114-1119 (2011).
15. Saravani H., Ghahfarokhi M.T. and Esmaeilzaei M.R. Synthesis and Characterization of Superparamagnetic $NiBaO_2$ Nano-Oxide Using Novel Precursor Complex $[Ba(H_2O)_8][Ni(dipic)_2]$. *J. Inorg. Organomet. Polym.* **26**: 660-666 (2016).
16. Tabatabaee M., Tahriri M., Tahriri M., Ozawa Y., Neumuller B., Fujioka H. and Toriumi K. Preparation, crystal structures, spectroscopic and thermal analyses of two co-crystals of $[M(H_2O)_6][M(dipic)_2]$ and $(atrH)_2[M(dipic)_2]$ (M = Zn, Ni, dipic = dipicolinate; atr = 3-amino-1H-1,2,4-triazole) with isostructural crystal systems. *Polyhedron* **33**: 336-340 (2012).
17. Nakamoto K. Infrared and Raman Spectra of Inorganic and Coordination Compounds. Wiley-Interscience, New York, (1997).
18. Shakirova O.G., Lavrenova L.G., Korotaev E.V., Kuratieva N.V., Kolokolov F.A. and Burdukov A.B. Structure and spin crossover in an iron (II) compound with tris(pyrazol-1-yl)methane and the complex $Eu(dipic)_2(Hdipic)]^{2-}$ anion. *J. Struct. Chem.* **57**: 471-477 (2016).
19. Siddiqi Z.A., Khalid M., Shahid M., Kumar S., Sharma P.K., Siddique A. and Anjuli. H-bonded supramolecular assembly via proton transfer: Isolation, X-ray crystallographic characterization and SOD mimic activity of $[Cu(dipic)_2]_2[PA\text{-}H]_4.5H_2O$. J. Mol. Struct. **1033**: 98-103 (2013).
20. Kirillova M.V., Kirillov A.M., DaSilva M.F.C.G., Kopylovich M.N., DaSilva J.J.R.F. and Pombeiro A.J.L. 3D Hydrogen Bonded Metal-Organic Frameworks Constructed from $[M(H_2O)_6][M'(dipicolinate)_2].mH_2O$ (M/M' = Zn/Ni or Ni/Ni). Identification of Intercalated Acyclic $(H_2O)_6/(H_2O)_{10}$ Clusters. *Inorg. Chim. Acta* **361**: 1728-1737 (2008).
21. Devereux M., McCann M., Leon V., McKee V. and Ball R.J. Synthesis and catalytic activity of manganese(II) complexes of heterocyclic carboxylic acids: X-ray crystal structures of $[Mn(pyr)_2]_n$, $[Mn(dipic)(bipy)_2]\cdot 4.5H_2O$ and $[Mn(chedam)(bipy)]\cdot H_2O$ (pyr=2-pyrazinecarboxylic acid; dipic=pyridine-2,6-dicarboxylic acid; chedam=chelidamic acid(4-hydroxypyridine-2,6-dicarboxylic acid); bipy=2,2-bipyridine). *Polyhedron* **21**: 1063-1071 (2002).
22. Kanthimathi M., Dhathathreyan A. and Nair B.V. Nanosized nickel oxide using bovine serum albumin as template. *Mater. Lett.* **58**: 2914–2917 (2004).
23. Morales M.R., Barbero B.P. and Cadús L.E. Evaluation and characterization of Mn – Cu mixed oxide catalysts for ethanol total oxidation: Influence of copper content. *Fuel* **87**: 1177-1186 (2008).
24. Yesilel O.Z., Ilker I., Refat M.S. and Ishida H. Syntheses and characterization of two copper pyridine-dicarboxylate compounds containing water clusters. *Polyhedron* **29**: 2345-2351 (2010).
25. Li P., Liu J., Nag N. and Crozier P.A. In situ preparation of Ni-Cu/TiO_2 bimetallic catalysts. *J. Catal.* **262**: 73-82 (2009).
26. Chen W., Lin M., Jiang T.L. and Chen M. Modeling and simulation of hydrogen generation from high-temperature and low-temperature water gas shift reactions. *Int. J. Hydrogen Energy* **33**: 6644-6656 (2008).